Journal of Catalysis 285 (2012) 145–151

Contents lists available at SciVerse ScienceDirect

Journal of Catalysis

journal homepage: www.elsevier.com/locate/jcat

Investigation of sulfur poisoning of CN_x oxygen reduction catalysts for PEM fuel cells

Dieter von Deak [a], Deepika Singh [a], Elizabeth J. Biddinger [a], Jesaiah C. King [a], Burcu Bayram [a], Jeffrey T. Miller [b], Umit S. Ozkan [a,*]

[a] Department of Chemical and Biomolecular Engineering, The Ohio State University, 140 W. 19th Avenue, Columbus, OH 43210, United States
[b] Chemical Sciences and Engineering Division, Argonne National Laboratory, Argonne, IL 60439, United States

ARTICLE INFO

Article history:
Received 18 March 2011
Revised 23 August 2011
Accepted 22 September 2011
Available online 22 October 2011

Keywords:
CN_x
X-ray absorption spectroscopy
Oxygen reduction
Sulfur poisoning
Active site

ABSTRACT

The role of the transition metal used during the growth of non-noble metal electrochemical oxygen reduction CN_x catalysts was investigated through sulfur treatment, a well-known poison for transition metal-based catalysts. The intent of sulfur poisoning was to show the existence of an electrocatalytic active site in CN_x that did not depend on iron. The sulfur treatment was shown to be effective on a platinum catalyst, as seen by the decreasing onset potential. The same treatment, however, not only showed no negative effect on the CN_x catalyst, but enhanced its performance, as seen by the increase in the onset potential. This suggests that, if there are iron-based active sites in these catalysts, they are either sulfur tolerant or they do not participate in the electrocatalytic oxygen reduction. The deposition of sulfur onto CN_x catalyst was verified by temperature-programmed oxidation and X-ray photoelectron spectroscopy. Iron K-edge X-ray absorption near edge structural analysis of the CN_x catalyst suggested that the iron phase, which was primarily composed of nanometer-sized metallic particles, was unchanged by sulfur poisoning, suggesting that the residual iron left in these materials is not catalytically accessible.

1. Introduction

Fuel cells have the potential to radically alter the contemporary energy landscape, but many economic and technological challenges must first be overcome. Economically prohibitive loadings of platinum are used in the proton exchange membrane (PEM) fuel cell cathodes to overcome the slow kinetics of the oxygen reduction reaction (ORR).

Non-noble metal catalysts have been shown to have significant oxygen reduction activity and could potentially reduce or replace platinum in PEM fuel cells. Research on oxygen reduction reaction over non-noble metal electrocatalysts was inspired by naturally occurring organic macrocycles in hemoglobin where oxygen adsorption readily occurs at low temperatures. In hemoglobin, oxygen adsorbs onto an iron center (heme site) that is coordinated by four surrounding nitrogen functional groups at 37 °C [1]. It was discovered that heme-like molecules, such as iron pthalocyanines and macrocycles, were active for ORR in the fuel cell cathode, but quickly deactivated in acidic environments where the Fe–N_x active sites are destroyed [2–5]. To improve the stability of these materials, pyrolysis, heat treatment in an inert atmosphere, above 600 °C was used to stabilize the organic macrocycles on a carbon support [3–15]. Although the pyrolysis step was found to completely destroy the coordinated metal active site, the catalyst materials prepared through pyrolysis were found to be more active and stable than macrocycles, leading researchers to believe that a new active site had been formed during the heat treatment [16]. The structure of this new active site has not been definitively determined, although researchers have hypothesized a number of different sites ranging from metal atoms stabilized by nitrogen groups, to non-metallic sites grown catalytically by the presence of a metal during pyrolysis [3,12,14,17–19].

The high-temperature treatment used to stabilize non-noble metal catalyst materials facilitates the formation of all possible bonding configurations, thereby allowing many atomic arrangements any of which could be responsible for the ORR activity. It has been established that a carbon source, a transition metal, and a nitrogen source need to be present during pyrolysis to achieve high ORR activity [17,20–31], but the exact bonding configuration that facilitates high ORR activity is still debated.

We have previously shown that significant ORR activity can be achieved in a metal-free (<1 ppm Fe) CN_x catalyst, and in light of those findings, it was suggested that iron was not a part of the active site, but plays the role of a growth catalyst for carbon nanostructures [32,33]. Although the presence of multiple active sites, i.e., one with a metallic center and one without, cannot be ruled out, the activity observed over these materials being solely due to the presence of Fe centers in very low concentrations (100 ppm or less) is less likely. If this were the case, the intrinsic activity of these metal centers would be exceptionally high. In this paper, we adopt an exclusionary approach by attempting to

* Corresponding author. Fax: +1 614 292 3769.
E-mail address: ozkan.1@osu.edu (U.S. Ozkan).

0021-9517/$ - see front matter © 2011 Elsevier Inc. All rights reserved.
doi:10.1016/j.jcat.2011.09.027

deliberately poison the catalysts with sulfur to determine whether a transition metal is present in the active site for oxygen reduction in CN_x materials. CN_x catalysts prepared using a number of different transition metals during synthesis have been shown to have significant activity with the CN_x catalyst grown on Fe- or Co-containing media having the highest activity [19,34–38]. Sulfur is a well-known catalyst poison, which has been shown to deactivate iron-based catalysts for Fischer–Tropsch, water-gas shift, ammonia synthesis, ammonia decomposition, and iron carburization [39–42]. Binding reaction of H_2S with the ferric center of heme has also been reported [1,43]. Similarly, hydrogen sulfide treatment can be expected to have a similar poisoning effect on any iron-containing active sites present on non-noble metal ORR electrocatalysts. To the best of our knowledge, this is the first time there have been any reports on the sulfur poisoning attempts of CN_x oxygen reduction catalysts.

2. Experimental

2.1. Materials synthesis

The CN_x growth media was prepared by incipient wetness impregnation of 2wt% Fe onto a nanopowder magnesia support (Sigma–Aldrich) using an aqueous solution of iron (II) acetate (Sigma–Aldrich), followed by drying of the growth media overnight at 110 °C in air. Two grams of growth media was then weighed into a quartz calcination boat and placed inside of a quartz calcination tube in a high-temperature furnace. The calcination tube was purged with nitrogen at 150 mL/min for 30 min and then heated at 10 °C/min until 900 °C was reached. Upon reaching 900 °C, acetonitrile (CH_3CN, Fisher, Optima grade)-saturated nitrogen gas at 150 mL/min was streamed over the growth media for 2 h. After the 2 h of catalyst growth treatment, the system was cooled under nitrogen to room temperature. The resulting carbon nanostructures were washed in 1 M HCl at 60 °C to remove the magnesia support and any exposed iron, rinsed with excess deionized and distilled water with vacuum filtration, and dried in a convection oven at 110 °C. The resulting dry material is considered nitrogen-containing carbon ORR catalyst (CN_x).

To study the effects of sulfur poisoning, CN_x was treated after catalyst growth in a variety of atmospheres. Between quartz wool plugs, 150 mg of CN_x was placed into a quartz reactor tube in a high-temperature furnace. The quartz tube was purged with nitrogen at 33 ml/min for 30 min and then heated at 10 °C/min until 350 °C was reached. At 350 °C, the catalyst was treated with 1050 ppm H_2S/N_2 or 5.7%H_2/N_2 at 33 ml/min for 2 h. At the end of 2 h of treatment, the system was cooled in nitrogen gas at 33 ml/min to room temperature. Control experiments were carried out over 20 wt.% Pt/Vulcan Carbon (BASF) that underwent the same treatment procedures.

2.2. Oxygen reduction activity testing

The ORR activity of catalysts was determined by electrochemical half-cell testing with a rotating disk electrode (RDE). Catalyst inks were prepared using a composition of 1:10:160 (by mass): catalyst: 5% Nafion in aliphatic alcohols: 100% ethanol. Inks were sonicated with low energy for 30 min. Three 5-μL aliquots of catalyst ink were applied to a 0.1642 cm^2 glassy carbon disk, resulting in a catalyst loading of 426 $\mu g/cm^2$. A model 636 RDE setup was connected to a Princeton Applied Research Bistat for the electrochemical testing. An Ag/AgCl (saturated KCl) reference electrode and a Pt wire counter electrode were used for the half-cell system. All reported potentials are referenced versus the normal hydrogen electrode (NHE). The half-cell electrolyte was 0.5 M H_2SO_4. It has been reported that there is no significant difference in ORR testing of CN_x catalysts between H_2SO_4 and $HClO_4$ solutions [11,44]. It should be noted that although H_2SO_4 is thought to poison platinum-based catalysts [45], since the electrochemical methods were identical for all Pt catalysts studied, the deactivation would be equivalent, making any activity differences attributable to the chemical treatments used.

ORR catalyst testing was performed using cyclic voltammetry (CV) on the glassy carbon disk. All CVs for CN_x were scanned from 1.2 V to 0.0 V to 1.2 V vs. NHE. The CVs for platinum were scanned from 1.2 V to 0.2 V to 1.2 V vs. NHE to prevent hydrogen evolution. To begin testing, the electrolyte was saturated with oxygen and disk CVs were run at 10 mV/s to remove any gaseous oxygen from the catalyst pores and fully wet the catalyst.

Prior to the collection of the background, the half-cell was purged with argon for 30 min to remove nearly all the dissolved oxygen. Disk CVs were run at a scan rate of 50 mV/s to eliminate impurities from the electrode surface. Immediately after the last scan, a disk CV was run at 10 mV/s while the assembly was rotating at 100 rpm to collect the background.

The electrolyte was, then, saturated with oxygen for 30 min to determine activity of the catalysts. Once again, disk CVs were run at a scan rate of 50 mV/s to eliminate impurities from the electrode surface. Immediately following the last scan, oxygen was bubbled through the electrolyte for 1–2 min to re-saturate the solution, following which a 1000 rpm oxygen-saturated electrolyte disk CV at 10 mV/s was performed. Additional CVs were run at 100 rpm and 0 rpm in oxygen-saturated electrolyte using a scan rate of at 10 mV/s.

To ensure that any possible contamination from Pt counter electrode did not affect the measurements taken in RDE apparatus, control experiments were performed where ORR activity of CN_x catalysts were measured in a RDE apparatus using a graphite counter electrode. The activity results did not show any change in activity, which could be ascribed to Pt contamination.

2.3. X-ray photoelectron spectroscopy

X-ray photoelectron spectroscopy (XPS) was used to examine the binding energies and environments of oxygen, nitrogen, carbon, and sulfur, when applicable, in the CN_x catalysts. A Kratos Ultra Axis Spectrometer with a monochromated aluminum anode source was used to collect a survey spectrum, O 1s, N 1s, C 1s, and S 2p regions for each CN_x catalyst sample. Analysis of the collected data was done on XPSPeak 4.1® using Shirley background for baseline correction and a combination of Lorentzian–Gaussian peaks for curve fitting. For quantitative comparison of the surface composition CN_x catalysts that underwent different treatments, the atomic sensitivity factors were used to correct the XPS peak areas for the relative sensitivity of the XPS instrument toward each species.

2.4. Temperature-programmed oxidation

Temperature-programmed oxidation (TPO) experiments were carried out using a mass spectrometer with gas chromatography interface (Thermo-Finnigan, Trace DSQ GC/MS, 2-1050 atomic mass units (amu)) to monitor the oxidation temperature and composition of the CN_x catalysts. For each run, 10 mg of CN_x catalyst was loaded into a quartz reactor tube with a quartz frit bed and was placed into a high-temperature, resistively-heated furnace (Carbolite, MTF 10/15/130), from which the exit stream was fed to the mass spectrometer. The temperature was ramped at 10 °C/min to 900 °C, while flowing 30 ml/min of 5% O_2/helium. Mass signal traces (m/z) from 12 to 80 amu were monitored during the experiment.

2.5. X-ray absorption spectroscopy

The X-ray absorption fine-structure spectroscopy (XAFS) measurements were taken on the bending magnet beam line of the Dow-Northwestern-Dupont Collaborative Access Team (DND-CAT, Sector 5) at the Advanced Photon Source, Argonne National Laboratory. EXAFS for the iron carbide sample used for comparison was collected at The Materials Research Collaborative Access Team (MRCAT, Sector 10) of the Advanced Photon Source, Argonne National Laboratory. Measurements were taken in the transmission mode with ionization chambers optimized for maximum current with linear response.

Standard procedures were used to extract the XAFS data from the absorption spectra using WINXAS97 software [46]. Samples were ground and cast into self-supporting pellets. The XAFS data were collected at room temperature in air.

2.6. Transmission electron microscopy

An FEI Tecnai F20 XT Transmission Electron Microscope (TEM) operated at 200 kV was used to locate the iron phase within the CN_x catalyst. The material was prepared for imaging by sonicating a suspension of catalyst in ethanol, which was then deposited on a lacey formvar–carbon supported on a 200 mesh copper TEM grid.

3. Results and discussion

3.1. Effect of H_2S on oxygen reduction activity

A hydrogen sulfide treatment was used to poison any iron-containing active sites present on CN_x catalysts. Pt/VC was also used for comparison. In previous reports, in the literature, it was shown that activity of Fe-containing CN_x materials was correlated with micropore volume (<2 nm), leading to the hypothesis that the ORR active site(s) was housed within Fe-/N-/C-type centers located in the micropores [47]. To effectively poison the proposed microporous Fe/N/C active site, the sulfur poison will need physical access to the sites while being chemically active. Oxygen has a collision diameter (σ_{O2}) of 3.467 Å, while hydrogen sulfide has a collision diameter (σ_{H2S}) of 3.623 Å [48]. This would suggest that hydrogen sulfide would have nearly the same micropore access as oxygen in CN_x catalyst. Furthermore, hydrogen sulfide is known to readily bind to the oxygen adsorption iron site in heme at 37 °C [1], and to poison Fe-based water gas shift catalysts in 300–450 °C range [42], so the H_2S treatment at 350 °C used in this study should be sufficient to bind and/or activate H_2S on the Fe-/N-/C-type active sites.

Oxygen reduction activity testing was carried out by cyclic voltammetry in a rotating disk electrode setup placed in an acidic solution to mimic the cathode environment in a direct methanol or hydrogen fuel cell. To isolate the heat treatment and reduction effects of H_2S poisoning, control experiments were carried out where separate samples of both CN_x and 20 wt.% Pt supported on Vulcan carbon were also heat-treated under the same conditions in a 5.7% H_2/N_2 atmosphere. Fig. 1 shows a comparison of the oxygen reduction activity of an untreated Pt/Vulcan carbon with the same catalyst that underwent different treatments, i.e., H_2 or H_2S, prior to the testing of the activities. The decrease in activity shown for the platinum catalyst verifies that the H_2S treatment has a detrimental effect on the ORR activity under the treatment conditions used in this study. The decrease in activity can be observed in the lower onset potential (i.e., higher over potential) compared with the untreated platinum catalyst, Fig. 1 (inset). This observation is not surprising since sulfur has been previously reported to poison platinum ORR catalysts [41,49]. The hydrogen treatment is seen to increase the onset potential over the Pt/VC

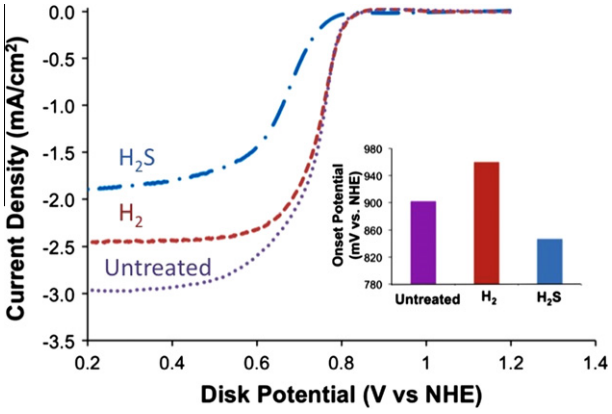

Fig. 1. Effect of H_2S treatment on the oxygen reduction activity of Pt/Vulcan carbon catalysts. Effect of H_2 treatment is also included as a control experiment. Inset: comparison of onset potential.

catalyst. This observation is consistent with the expectation that reduced platinum sites would be more active for ORR. This control experiment with H_2 also showed that any decrease in activity cannot be attributed to a heating effect. The differences in the limiting current could be due to the chemical treatment, affecting the coarseness or porosity of electrodes [50].

The experiments carried out with Pt catalysts were important in showing that the H_2S treatment was sufficient to impart a measurable poisoning effect, and thus validating the use of a similar procedure for CN_x catalysts.

Fig. 2 shows similar linear polarization curves for the untreated CN_x and catalysts that were treated under different atmospheres, i.e., H_2 or H_2S, prior to activity testing. The inset shows a comparison of the onset potentials. The sulfur poisoning treatment was found not to decrease the activity of CN_x oxygen reduction catalyst. On the contrary, CN_x ORR current density and onset potential were found to improve with H_2S treatment (Fig. 2). The greater current density suggests that electrode porosity or surface coarseness may have been altered by the H_2S treatment, allowing for increased mass transfer during oxygen reduction; however, the improved onset potential (i.e., lower over potential) demonstrates improved intrinsic activity. The H_2 treatment in the control experiment also led to a higher onset potential, but the improvement was much more pronounced with H_2S treatment. This suggests that a secondary heat treatment in a reducing atmosphere can increase the activity of CN_x. The fact that there was no loss of activity

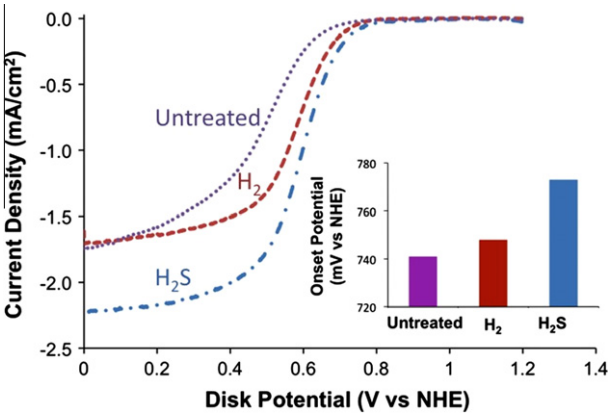

Fig. 2. Effect of H_2S treatment on the oxygen reduction activity of CN_x catalysts. Effect of H_2 treatment is also included as a control experiment. Inset: comparison of onset potential.

following a treatment in H_2S is significant in showing that, if an iron-containing active site is present, either it is sulfur tolerant or does not participate in the electrocatalytic oxygen reduction. This result is not surprising considering it has already been shown that sulfur compounds introduced during pyrolysis could enhance CN_x catalyst growth, while the oxygen reduction activity remained largely unchanged [51]. Although it is not clear why an enhancement in CN_x ORR activity was observed with H_2S treatment, Chung et al. reported a similar activity increase on a non-precious metal catalyst synthesized by pyrolyzing cyanamide and iron sulfate [52]. If N-sites incorporated into the carbon nanostructure have ORR activity, it is conceivable that other heteroatoms such as sulfur can fulfill a similar role. The incorporation of heteroatoms such as phosphorus and sulfur into graphite has been demonstrated both experimentally and theoretically [53,54], and results suggesting ORR activity of other heteroatom-containing carbon structures have been reported [51,55–57]. The electronic structure calculations reported earlier [53] suggest an increased curvature in the graphite plane, due to heteroatom substitution. If the sulfur incorporation took place in the basal plane, one would expect such a "corrugation," leading to a more defect-prone structure. It is also conceivable that the heteroatom substitution takes place at the edge sites, e.g., sulfur-occupying sites analogous to pyridinic nitrogen. At this point, it is not clear whether sulfur is replacing edge nitrogen or incorporating additional heteroatoms, and hence, changing the electron donor characteristics of graphite.

3.2. X-ray photoelectron spectroscopy

CN_x catalysts that underwent heat treatment under different atmospheres were further characterized with XPS and temperature-programmed oxidation experiments to investigate the effect of such treatments on the surface and bulk properties of these catalysts and to determine the extent and location of sulfur incorporation to the carbon phase of the CN_x catalysts. The sulfur poisoning of the iron phase in CN_x catalyst was further studied by X-ray absorption spectroscopy.

Iron and magnesium were not detectable in the survey scans of any of the CN_x catalysts studied. This finding is consistent with our previous reports [58] and suggests that the acid washing step for CN_x fabrication removed most of the surface iron and magnesia. The XPS analysis of CN_x catalysts found similar nitrogen species surface compositions, regardless of the treatment (Fig. 3). Fig. 4 shows a comparison of the X-ray photoelectron spectra in the S 2p region for an H_2S-treated and an untreated CN_x catalyst. Although the intensity in this region is low due to the low intrinsic atomic sensitivity of the instrument for sulfur, photoelectron peaks arising from the presence of sulfur species can be seen in the S 2p envelope for the H_2S-treated catalyst. Deconvolution for providing insights to the nature and relative surface concentration of sulfur species was difficult due to weakly resolved envelope. However, it is possible to discern three different photoelectron peaks located at 161 eV, 165 eV, and 169 eV, which can be associated with sulfur species in sulfide (S^{2-}), sulfite (SO_3^{2-}), sulfate (SO_4^{2-}) environments, respectively [59]. It should be noted that the splitting between $2p_{3/2}$ and $2p_{1/2}$ was not observed for the S 2p envelope due to small spin orbit splitting for sulfur (1.18 eV). Formation of sulfite and sulfate species can be associated with interaction of adsorbed sulfur with oxygen from ambient air during sample transfer, although an interaction between the sulfur- and the oxygen-containing functional groups present on the CN_x catalysts, leading to formation of sulfite species cannot be ruled out.

The elemental surface compositions of the CN_x samples determined from the quantitative analysis of XPS data are presented in Table 1. The results showed a redistribution of the elemental

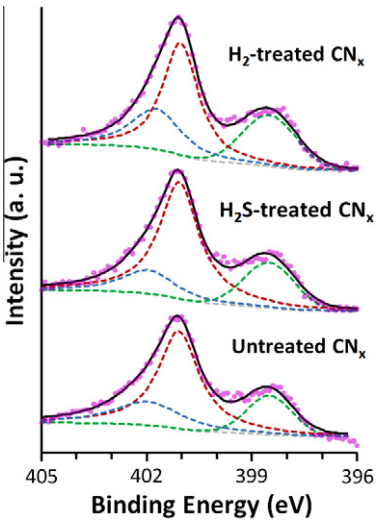

Fig. 3. X-ray photoelectron spectra in the N 1s region for untreated and heat-treated CN_x catalysts under different atmospheres.

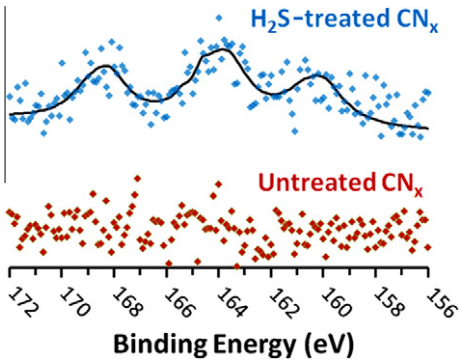

Fig. 4. X-ray photoelectron spectra of the S 2p region for untreated and H_2S-treated CN_x catalysts under different atmospheres.

surface concentration with H_2S treatment. The relative amount of surface oxygen was less for CN_x catalysts exposed to a reducing treatment. The reducing atmosphere used in H_2 and H_2S treatments can account for this change. The relative amounts of different N species were also seen to change in favor of pyridinic nitrogen. However, small amount of sulfur was also detected on the surface of H_2S-treated sample. There have been previous reports suggesting that changes in the oxygen [60] and nitrogen [24,61] surface species can affect ORR electrocatalytic activity. It is difficult to discern which of these changes, if any, have contributed to the improved performance. It is possible that there may be multiple factors contributing to the change in activity, such as increase in relative surface concentrations of edge nitrogen sites as well as incorporation of sulfur atoms in the graphite matrix. Especially, the latter would be expected to change the electron donor characteristics of carbon. It should also be noted that the change in the performance of CN_x catalysts does not only manifest itself through the improved onset potential, but also through the increased limiting current. The latter can be attributed to changes in the textural properties, hence mass transfer characteristics, of the catalyst. It is possible that the H_2S treatment could lead to defects in the graphite structure due to the larger size disparity between the carbon and the sulfur. It is also conceivable that H_2S could lead to increased pore volumes that would enhance the mass transfer characteristics [62,63].

Table 1
Compositional analysis of CN_x catalysts from X-ray photoelectron spectroscopy.

	O 1s (%)	N 1s (%)			C 1s (%)	S 2p (%)
	532.9 eV	398.8 eV	401.2 eV	402.0 eV	200.1 eV	163.5 eV
Untreated	3.8	1.4	4.5	1.7	88.6	0.0
H_2S treated	2.4	1.7	3.5	0.9	91.3	0.2
H_2 treated	2.7	1.8	3.8	1.9	89.8	0.0

3.3. Temperature-programmed oxidation

Temperature-programmed oxidation experiments were carried out over the untreated CN_x catalyst as well as catalysts that were heat-treated under different atmospheres (Fig. 5). Regardless of the pretreatment conditions, the CO_2 ($m/z = 44$) and NO_2 ($m/z = 46$) traces closely followed each other and broad evolution bands for these species, which are associated with the decomposition of the CN_x structure, were observed in 510–720 °C region. Over the H_2S-treated catalyst, evolution of SO_2 ($m/z = 64$) that is concomitant to CO_2 and NO_2 was observed. This indicates that sulfur species that were retained on the surface after the H_2S pretreatment were strongly bonded to the surface rather than being physically adsorbed.

3.4. X-ray absorption spectroscopy

Since a transition metal improves the pyrolic formation of the non-noble metal active site, it is difficult to ascertain the role of iron in ORR activity. X-ray absorption spectroscopy was used to probe the local bonding environment of the iron in CN_x oxygen reduction catalysts. The XANES spectra for all CN_x catalysts, Fig. 6, were nearly identical regardless of the post-synthesis treatment conditions, indicating that the local Fe structure is unchanged by H_2S treatment. All CN_x XANES spectra appeared to strongly resemble iron in the metallic or carbide phase, Fig. 7. None of the CN_x samples studied resembled the iron phthalocyanine standard, which is similar to the nitrogen-bonded transition metal active site proposed by some researchers [19,64,65]. TEM of CN_x catalysts revealed iron entirely encased within several carbon sheets, Fig. 7, inset. Since the iron phase is isolated from the chemical treatments by layers of carbon, it is not surprising that the Fourier transform obtained at the Fe K-edge and k^2-weighted EXAFS displayed a nearly identical local bonding environment for untreated and H_2S-treated CN_x, Fig. 8. The iron contained within CN_x has a small metallic phase and an iron phase bonded to a lighter element (nitrogen, oxygen, and/or carbon). It can be seen that

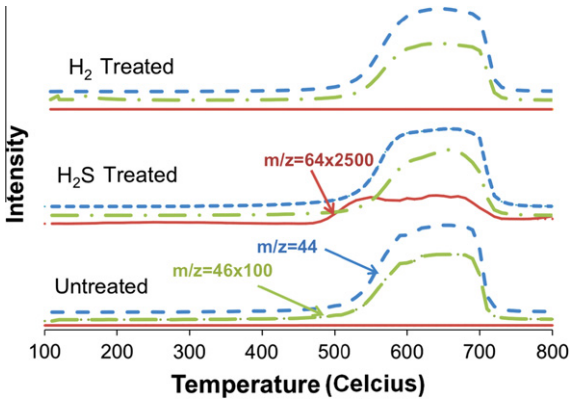

Fig. 5. Evolution of CO_2 ($m/z = 44$ amu), NO_2 ($m/z = 46$ amu), and SO_2 ($m/z = 64$ amu) as a function of temperature during temperature-programmed oxidation of untreated, H_2S-, N_2-, and H_2-treated CN_x.

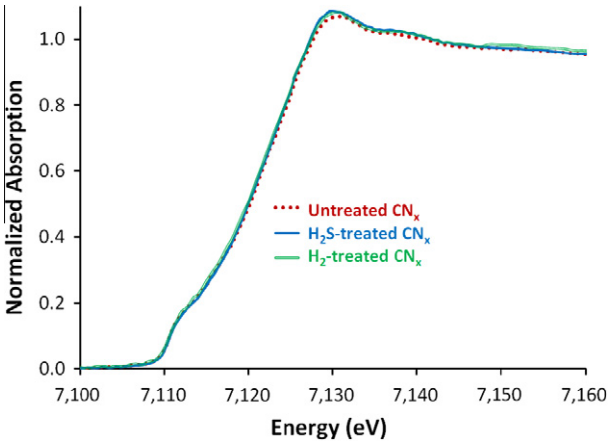

Fig. 6. XANES Fe K-edge spectra for untreated, H_2S-, and H_2-treated CN_x.

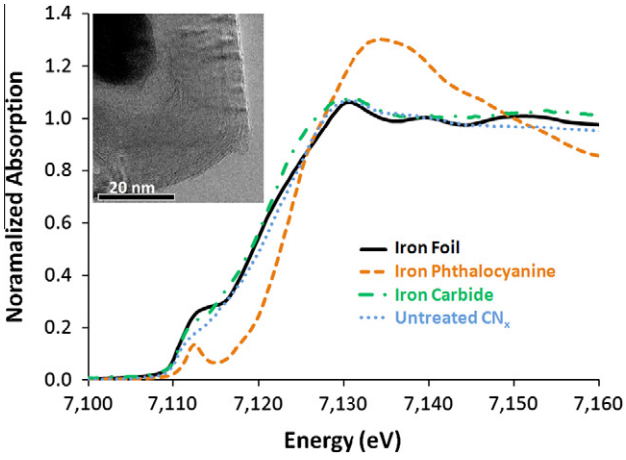

Fig. 7. XANES Fe K-edge spectra for, iron foil, iron phthalocyanine, iron carbide and untreated CN_x.

untreated CN_x Fe-Fe bond length is less than that of bulk iron, Fig. 9. This is likely due iron particles being much smaller in CN_x catalyst than of a bulk iron foil. The iron–iron bonding shoulder at ~1.5 Å in CN_x catalyst coincides with Fe–N bond distance in iron phthalocyanine, but also aligns with the Fe–C bond distance in iron carbide. Due to the similar scattering spectra of 2p elements, it cannot be determined whether the CN_x peak at ~1.5 Å is due to an iron nitrogen, carbon, or oxygen bond. The EXAFS for iron carbide displayed the same peak structure and locations as the CN_x catalysts studied. This is in agreement with an investigation into the CN_x iron phase through Mössbauer spectroscopy, which revealed iron to consist of a metallic phase (a paramagnetic γ-Fe phase, which would be unstable in air) and a cementite phase (Fe_3C), which is likely to be formed during the carbon fiber growth [58]. Working iron catalysts are often a complex mixture of iron

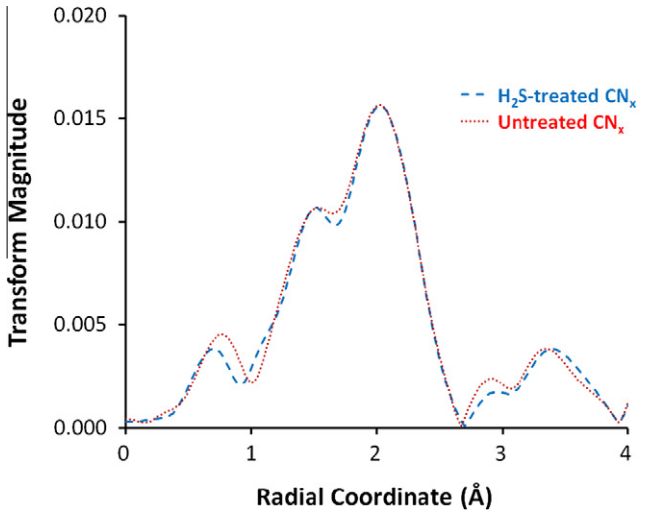

Fig. 8. EXAFS Fe K-edge spectra for H_2S-treated and untreated CN_x.

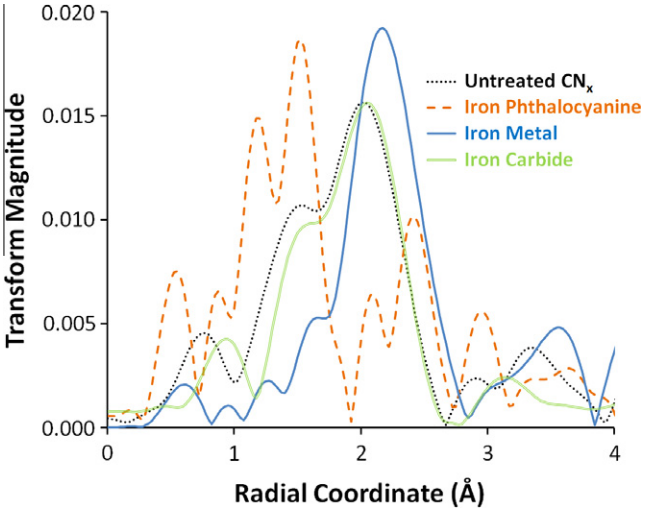

Fig. 9. EXAFS Fe K-edge spectra for untreated CN_x, iron phthalocyanine, iron metal, and iron carbide.

carbide compounds, often containing a fraction of iron oxides [66]. An EXAFS theoretical structural model was prepared by Jacobs et al. using *ab initio* multiple scattering calculations of X-ray absorption fine structure for cementite (Fe_3C), Hägg carbide (Fe_5C_2), ε-carbide (Fe_3C), and η-carbide (Fe_2C) to generate the Fourier transform magnitude versus bond distance for the iron K-edge in order to characterize the iron carbides present in Fischer–Tropsch synthesis catalysts [66]. CN_x oxygen reduction electrocatalyst resembles a combination of the ε-carbide (Fe_3C) and Hägg carbide (Fe_5C_2) when compared to the simulated carbide EXAFS spectra. Although CN_x catalysts are grown in a reducing atmosphere, the presence of iron oxides cannot be ruled out.

4. Conclusions

A sulfur poisoning treatment was performed on both platinum and CN_x oxygen reduction catalysts to investigate the role of the transition metal in the CN_x ORR active site. The intent of sulfur poisoning treatment was to effectively eliminate iron from the proposed electrocatalytic oxygen reduction active sites of CN_x. The sulfur treatment was found to reduce ORR activity on the platinum catalyst, which demonstrated the validity of the sulfur poisoning treatment. The H_2S treatment was found to increase the activity on the CN_x catalyst. The incorporation of sulfur into the CN_x catalyst was verified by TPO and XPS spectra. The iron phase within the CN_x catalysts was investigated with X-ray absorption and was found to be similar for the treatments studied, suggesting that iron was not catalytically accessible. XANES analysis of the CN_x Fe K-edge showed the iron phase in CN_x to be mostly metallic with possible contributions from a carbidic phase. No spectra resembled the iron macrocycle standard, which is similar to the hypothesized nitrogen-bonded transition metal ORR active site.

The source of the increase in ORR activity observed over the CN_x catalyst following H_2S treatment is not clear, but it may be due to multiple factors, including creation of new active sites associated with sulfur or creation of defects in the graphite matrix due to size disparity between carbon and sulfur. It is also likely that the H_2S treatment may be changing the mass transfer characteristics of the catalyst by increasing porosity, and hence changing the limiting current.

Acknowledgments

The authors acknowledge the financial support for this work from US Department of Energy Basic Energy Sciences through the Grant DE-FG02-07ER15896. Portions of this work were performed at the DuPont-Northwestern-Dow Collaborative Access Team (DND-CAT) located at Sector 5 of the Advanced Photon Source (APS). DND-CAT is supported by E.I. DuPont de Nemours & Co., The Dow Chemical Company and the State of Illinois. Use of the APS was supported by the US Department of Energy, Office of Science, Office of Basic Energy Sciences, under Contract No. DE-AC02-06CH11357. The authors also acknowledge the NSF support for acquisition of the XPS system under NSF-DMR Grant #0114098.

References

[1] B. Alberts, A. Johnson, J. Lewis, M. Raff, K. Roberts, P. Walter, Molecular Biology of the Cell, fourth ed., Garland Science, New York, 2002.
[2] H. Jahnke, M. Schonborn, G. Zimmerman, Fortschr. Chem. Forsch. 61 (1976) 133.
[3] K. Wiesener, Electrochim. Acta 31 (1986) 1073.
[4] E. Yeager, Electrochim. Acta 29 (1984) 1527.
[5] E. Yeager, J. Mol. Catal. 38 (1986) 5.
[6] A.L. Bouwkamp-Wijnoltz, W. Visscher, J.A.R. van Veen, E. Boellaard, A.M. van der Kraan, S.C. Tang, J. Phys. Chem. B 106 (2002) 12993.
[7] A.L. Bouwkamp-Wijnoltz, W. Visscher, J.A.R. van Veen, S.C. Tang, Electrochim. Acta 45 (1999) 379.
[8] M. Bron, S. Fletcher, M. Hilgendorff, P. Bogdanoff, J. Appl. Electrochem. 32 (2002) 211.
[9] M. Bron, J. Radnik, M. Fieber-Erdmann, P. Bogdanoff, S. Fiechter, J. Electroanal. Chem. 535 (2002) 113.
[10] G. Faubert, R. Cote, D. Guay, J.P. Dodelet, G. Denes, P. Bertrand, Electrochim. Acta 43 (1998) 341.
[11] S. Gojkovic, S. Gupta, R. Savinell, J. Electroanal. Chem. 462 (1999) 63.
[12] P. Gouerec, A. Biloul, O. Contamin, G. Scarbeck, M. Savy, J. Riga, L.T. Weng, P. Bertrand, J. Electroanal. Chem. 422 (1997) 61.
[13] P. Gouerec, A. Biloul, O. Contamin, G. Scarbeck, M. Savy, J.M. Barbe, R. Guilard, J. Electroanal. Chem. 398 (1995) 67.
[14] D. Scherson, A.A. Tanaka, S.L. Gupta, D. Tryk, C. Fierro, Z. Holze, E.B. Yeager, Electrochim. Acta 31 (1986) 1247.
[15] J.A.R. van Veen, J.F. van Baar, K.J. Kroese, Chem. Soc. Faraday Trans. I 77 (1981) 2827.
[16] P. Gouerec, M. Savy, Electrochim. Acta 44 (1999) 2653.
[17] F. Jaouen, S. Marcotte, J.-P. Dodelet, G. Lindbergh, J. Phys. Chem. B 107 (2003) 1376.
[18] F. Jaouen, M. Lefevre, J.-P. Dodelet, M. Cai, J. Phys. Chem. B 110 (2006) 5553.
[19] T.S. Olson, S. Pylypenko, J. Fulghum, P. Atanassov, J. Electrochem. Soc. 157 (2010) B54.
[20] G. Faubert, R. Cote, D. Guay, J.P. Dodelet, G. Denes, C. Poleunis, P. Bertrand, Electrochim. Acta 43 (1998) 1969.
[21] J. Fournier, G. Lalande, R. Cote, D. Guay, J.P. Dodelet, J. Electrochem. Soc. 144 (1997) 218.
[22] S. Gupta, D. Tryk, I. Bae, W. Aldred, E. Yeager, J. Appl. Electrochem. 19 (1989) 19.

[23] R. Cote, G. Lalande, D. Guay, J.P. Dodelet, G. Denes, J. Electrochem. Soc. 145 (1998) 2411.
[24] G. Lalande, R. Cote, D. Guay, J.P. Dodelet, L.T. Weng, P. Bertrand, Electrochim. Acta 42 (1997) 1379.
[25] M. Lefevre, J.P. Dodelet, P. Bertrand, J. Phys. Chem. B 104 (2000) 11238.
[26] M. Lefevre, J.P. Dodelet, P. Bertrand, J. Phys. Chem. B 106 (2002) 8705.
[27] H. Wang, R. Cote, G. Faubert, D. Guay, J.P. Dodelet, J. Phys. Chem. B 103 (1999) 2042.
[28] G. Faubert, R. Côté, J.P. Dodelet, M. Lefèvre, P. Bertrand, Electrochim. Acta 44 (1999) 2589.
[29] M. Lefevre, J.-P. Dodelet, Electrochim. Acta 48 (2003) 2749.
[30] D. Villers, X. Jacques-Bedard, J.P. Dodelet, J. Electrochem. Soc. 151 (2004) A1507.
[31] S. Ye, A.K. Vijh, Electrochem. Commun. 5 (2003) 272.
[32] P.H. Matter, U.S. Ozkan, Catal. Lett. 109 (2006) 115.
[33] P.H. Matter, E. Wang, M. Arias, E.J. Biddinger, U.S. Ozkan, J. Phys. Chem. B 110 (2006) 18374.
[34] J.-H. Kim, A. Ishihara, S. Mitsushima, N. Kamiya, K.-I. Ota, Electrochim. Acta 52 (2007) 2492.
[35] B.R. Limoges, R.J. Stanis, J.A. Turner, A.M. Herring, Electrochim. Acta 50 (2005) 1169.
[36] J.-i. Ozaki, S.-i. Tanifuji, A. Furuichi, K. Yabutsuka, Electrochim. Acta 55 (2010) 1864.
[37] P.H. Matter, E.J. Biddinger, U.S. Ozkan, in: J.J. Spivey (Ed.), Catalysis, the Royal Society of Chemistry, Cambridge, UK, 2007, p. 338.
[38] P.H. Matter, E. Wang, U.S. Ozkan, J. Catal. 243 (2006) 395.
[39] W. Arabczyk, D. Moszynski, U. Narkiewicz, R. Pelka, M. Podsiadly, Catal. Today (2007) 43.
[40] J. Oudar, Catalysis Reviews: Science and Engineering 22 (1980) 171.
[41] Y. Garsany, O.A. Baturina, K.E. Swider-Lyons, J. Electrochem. Soc. 156 (2009) B848.
[42] L. Zhang, J.M.M. Millet, U.S. Ozkan, J. Mol. Catal. A – Chem. 309 (2009) 63.
[43] R. Pietri, A. Lewis, G.R. Leon, G. Casabona, L. Kiger, S.-R. Yeh, S. Fernandez-Alberti, M.C. Marden, C.L. Cadilla, J. Lopez-Garriga, Biochemistry 48 (2009) 4881.
[44] F. Jaouen, J. Herranz, M. Lefevre, J.-P. Dodelet, U.I. Kramm, I. Herrmann, P. Bogdanoff, J. Maruyama, T. Nagaoka, A. Garsuch, J.R. Dahn, T.S. Olson, S. Pylypenko, P. Atanassov, E.A. Ustinov, ACS Appl. Mater. Interf. 1 (2009) 1623.
[45] K.-L. Hsueh, E.R. Gonzalez, S. Srinivasan, Electrochim. Acta 28 (1983) 691.
[46] T. Ressler, J. Phys. IV 7 (1997) C2.
[47] S. Barazzouk, M. Lefevre, J.-P. Dodelet, J. Electrochem. Soc. 156 (2009) B1466.
[48] E.L. Cussler, Diffusion Mass Transfer in Fluid Systems, second ed., Cambridge University Press, New York, 1997.
[49] Y. Garsany, B.D. Gould, O.A. Baturina, K.E. Swider-Lyons, Electrochem. Solid-State Lett. 12 (2009) B138.
[50] H. Yang, N. Alonso-Vante, C. Lamy, D.L. Akins, J. Electrochem. Soc. 152 (2005) A704.
[51] E.J. Biddinger, D.S. Knapke, D. von Deak, U.S. Ozkan, Appl. Catal. B – Environ. 96 (2010) 72.
[52] H.T. Chung, C.M. Johnston, K. Artyushkova, M. Ferrandon, D.J. Myers, P. Zelenay, Electrochem. Commun. 12 (2010) 1792.
[53] B.G. Sumpter, J. Huang, V. Meunier, J.M. Romo-Herrera, E. Cruz-Silva, H. Terrones, M. Terrones, Int. J. Quantum Chem. 109 (2009) 97.
[54] R.R.V.A. Rios, D.E. Alves, I. Dalmazio, S.F.V. Bento, C.L. Donnici, R.M. Lago, Mater. Res. 6 (2003) 129.
[55] M.P. Woods, E.J. Biddinger, P.H. Matter, B. Mirkelamoglu, U.S. Ozkan, Catal. Lett. 136 (2010) 1.
[56] D. von Deak, E.J. Biddinger, K.A. Luthman, U.S. Ozkan, Carbon 48 (2010) 3637.
[57] X. Bao, D. von Deak, E. Biddinger, U.S. Ozkan, C.M. Hadad, Chem. Commun. 46 (2010) 8621.
[58] P.H. Matter, E. Wang, J.-M.M. Millet, U.S. Ozkan, J. Phys. Chem. C 111 (2007) 1444.
[59] J.F. Moulder, W.F. Strickle, P.E. Sobol, K.D. Bomben, Handbook of Photoelectron Spectroscopy, Perkin-Elmer Corporation, Eden Prairie, MN, 1992.
[60] V.V. Strelko, N.T. Kartel, I.N. Dukhno, V.S. Kuts, R.B. Clarkson, B.M. Odintsov, Surf. Sci. 548 (2004) 281.
[61] P.H. Matter, E. Wang, M. Arias, E.J. Biddinger, U.S. Ozkan, J. Mol. Catal. 264 (2007) 73.
[62] F. Jaouen, E. Proietti, M. Lefevre, R. Chenitz, J.P. Dodelet, H.T. Chung, C.M. Johnston, P. Zelenay, Energy Environ. Sci. 4 (2011) 114.
[63] M. Lefevre, J.-P. Dodelet, Electrochim. Acta 53 (2008) 8269.
[64] M. Lefevre, E. Proietti, F. Jaouen, J.-P. Dodelet, Science 324 (2009) 71.
[65] J. Maruyama, I. Abe, J. Electrochem. Soc. 154 (2007) B297.
[66] G. Jacobs, A. Sarkar, B.H. Davis, D. Cronauer, A.J. Kropf, C.L. Marshall, in: B.H. Davis, M.L. Occelli (Eds.), Advances in Fischer-Tropsch Synthesis Catalysts and Catalysis, CRC Press, 2009, p. 119.